



Absorbance Linearity and Repeatability in Cylindrical Internal Reflectance FT-IR Spectroscopy of Liquids

Walter M. Doyle¹

This paper reports the results of a program aimed at eliminating the sources of performance variability and excessive nonlinearity that have limited the effectiveness of the cylindrical internal reflectance technique for use in quantitative FT-IR analysis. After discussing the various optical factors that can affect performance, it describes a new adjustment-free optical design which promises to eliminate those factors which lead to data unpredictably. Finally, it summarizes the results of a series of experiments carried out to test the effectiveness of the new design. These confirm the achievement of three significant improvements: an enhancement of band strengths by factors of typically 2.5 to 3, significantly improved absorbance linearity, and a high degree of data repeatability under varied experimental conditions.

1. Background

Over the past several years, internal reflectance spectroscopy has become widely used as a practical and convenient method for the infrared spectral analysis of liquids. In particular, IR accessories employing circular cross section “cylindrical” internal reflection elements have found broad acceptance. This is largely due to their compatibility with reliable and convenient O-ring seals, advantageous fluid dynamic properties, and compatibility with the circular cross-section IR beam of the typical FT-IR spectrometer.¹

During this same period, there has been recurring concern regarding the extent to which cylindrical internal reflectance (CIR) spectroscopy could be relied on for quantitative analysis.² This concern has been addressed by a detailed study of Braue and Pannella in which mixtures of acetone and water were analyzed in five sets of three runs each over a four-month period.³ Although these authors concluded that quantitative analysis of aqueous solutions is possible with commercial CIR cells, they did note some significant limitations, including severe nonlinearity of peak height measurements and a marked dependence of measurement results on positioning of the internal reflectance element. This later problem implies a need for very careful adjustment in order to obtain reproducible data. The purpose of the present study has been to determine

the extent to which an optimized optical design would result in improved absorbance linearity and repeatability and eliminate the need for precise adjustment.

Several factors can lead to nonlinearity in internal reflectance spectral measurements. Not least of these is the fact that the process itself becomes highly nonlinear at very high absorbance values.⁴ Other sources of nonlinearity include chemical interactions and limited instrument resolution³ as well as data processing approximations in the handling of transmittance values near zero, dependence of refractive index on chemical composition, polarization dependence, and finally, dependence of effective sample thickness on the angle of incidence of the IR radiation. My analysis indicates not only that this last factor can be a major contributor to nonlinearity but also that it can lead to unpredictable variations in performance with changes in the experimental geometry. The present program has thus been primarily concerned with understanding and minimizing these effects.

2. Optical Sources of Error in Internal Reflectance Spectroscopy

Distribution of Incidence Angles and Number of Reflections at the Sample Interface. The internal reflection phenomenon is inherently dependent on angle of incidence of the radiation at the interface between the internal reflectance element and the analyte. The magnitude of this dependence is illustrated by Fig. 1, a set of computer-generated curves of effective sample thickness as a function of angle of incidence. As these curves

¹The author is with Hellma Axiom, 1451-A Edinger Ave, Tustin, California 92780. W.M. Doyle's e-mail address is michael.doyle@hellma.com.

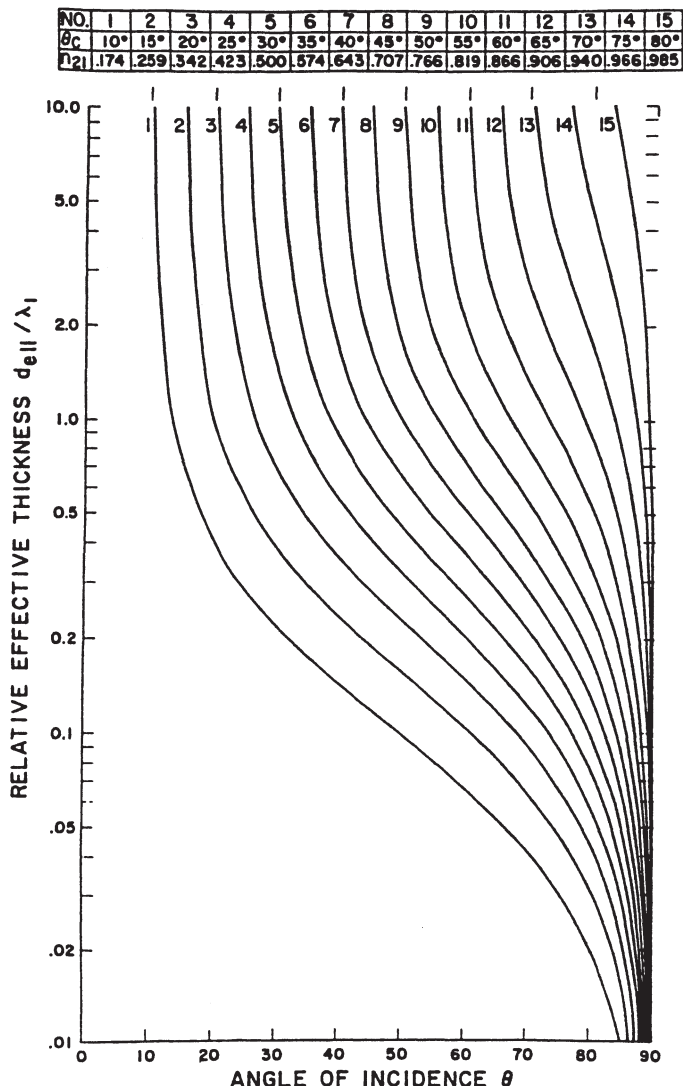


Fig. 1: Curves of relative effective thickness vs. angle of incidence at the analyte interface for polarization parallel to the plane of incidence. n_{21} is the ratio of the analyte refractive index to the IRE refractive index (i.e., $n_{21} = 2_2/n_1$). θ_c is the critical angle for each ratio. This figure has been reproduced, with permission, from N.J. Harrick, Internal Reflection Spectroscopy (Ref. 4)

reveal, a 10° change in incidence angle can easily lead to a factor-of-two change in effective sample thickness and hence in measured absorbance. If radiation covering a range of angles is used, the results will be analogous to those obtained with a wedged cell in transmission spectroscopy. As Hirschfeld has discussed in detail, this situation gives rise to a nonlinear dependence of measured absorbance on concentration.⁵ In the case of the wedged cell, the data can be corrected if the wedge angle is known. This is not the case in internal reflectance spectroscopy, since the dependence of effective thickness on angle is both nonlinear and dependent on the refractive index of the analyte and since the angular distribution of optical rays will generally not be well characterized. Thus, to maximize the linearity of internal reflectance data, it is necessary to minimize the angular spread of rays traveling through the

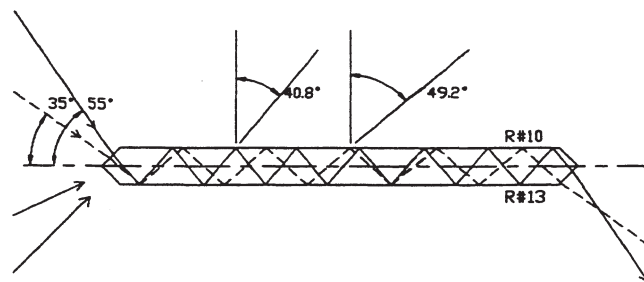


Fig. 2. Optical schematic of a CIR cell using sharply focused IR radiation. The rays included are the extreme rays which would normally come to a focus on the axis of the system in the absence of the internal reflection element (IRE). This figure illustrates the wide range of incidence angles at the analyte interface, the range in number of reflections from ten to thirteen, the spherical aberration caused by the presence of the IRE in the focal region, and the lack of correlation between ray direction and position at the output of the IRE.

internal reflectance element.

The CIR cell used by Braue and Pannella in the study mentioned above employed focused radiation striking the element at angles ranging from 35 to 55° from the axis. With the ZnSe element used, this spread would result in incidence angles from 40.8 to 49.2° at the interface between the analyte and the element, as illustrated in Fig. 2. This range is sufficient to give rise to more than a 50% variation of effective sample thicknesses. In addition, those rays which have the lower incidence angles are not only more strongly absorbed at each reflection but also experience a greater number of reflections. These two interrelated effects combine to give rise to a strong dependence of absorbance on incidence angle. As noted above, we would expect this result in significant nonlinearity.

Figure 2 also illustrates the fact that, with the wide range of angles employed, there is little correlation between the angle of propagation of a ray and its position on exiting the rod. As a result, any movement of the internal reflectance element or the output collecting optics relative to each other can lead to selective and unpredictable vignetting of the angular distribution of rays. For example, the two rays used for illustration in Fig. 2 exit the rod at widely separated points. It is doubtful that any adjustment of the collecting optics would be able to image both of these rays on the IR detector simultaneously.

This effect is enhanced to the extent that the end of the rod is larger than the image of the detector. However, even in the case of the 3-mm-diameter rod used by Braue and Pannella³, we would expect to see a random change in the average effective sample thickness and hence in the absorbance linearity and calibration of the system whenever the adjustment of the collecting optics is changed.

Optical Aberrations and Skew Ray Effects. The accuracy of CIR measurements can also be limited by aberrations which alter the distribution of optical rays in the cell in an unpredictable fashion. Two sources of aber-

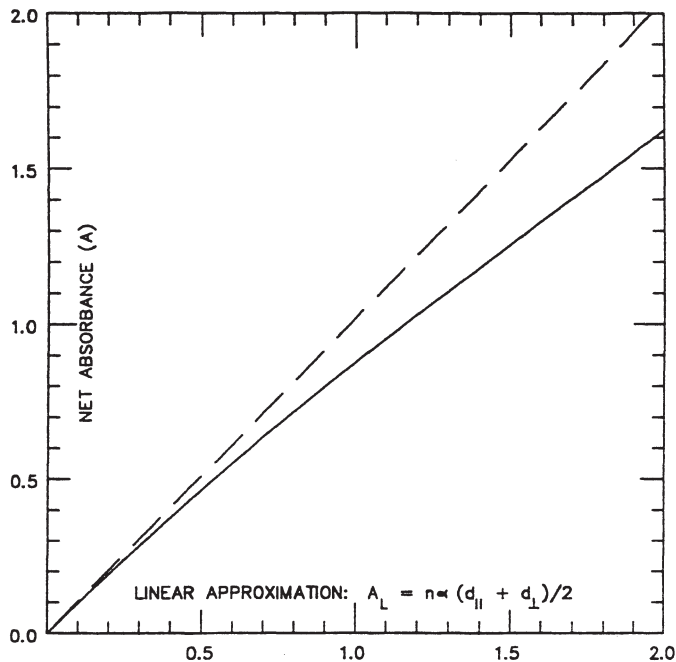


Fig 3. Predicted absorbance functionality for randomly polarized radiation, assuming a factor-of-two difference between the effective sample thickness for the parallel and perpendicular polarization components (i.e., $d_{\parallel} = 2d_{\perp}$). This ratio is approximately correct for a wide range of refractive index values at 45° incidence. The straight dashed line corresponds to Beer's law.

rations exist in the device used by Braue and Pannella: the internal reflectance element (IRE) itself and the reflexicon optics used to couple light in and out of the IRE.³

The first source of difficulty occurs because the IRE is positioned in a sharply focused beam. The problem can be easily understood if we think of the IRE as being equivalent to a thick plate inserted in the focal region of the optics. In any optical system, this would lead to severe spherical aberration. This effect can be seen by observing the paths of the two rays shown in Fig. 2. Rather than coming to a focus on axis as they would without the IRE, these rays cross considerably below the axis. This effect works in tandem with the variation in number of reflections with angle (discussed above) to thwart any attempt to image light through the IRE. As a result, we would expect a cell using a large-diameter rod to exhibit inferior performance to one using a small rod, which more nearly approximates a light pipe.

The second source of aberrations is the use of aspheric reflexicon optics to couple the radiation into and out of the IRE. Reflexicon optical systems are ideally suited for applications involving well-collimated coherent radiation, such as combining the outputs of several high-power lasers⁶. However, these systems exhibit severe coma when used with incoherent radiation. One result of this response is a tendency to increase the divergence of skew rays, exacerbating the effects to be discussed in the following paragraph.

The discussion above, in the section preceding this one, sug-

gests that the performance limitations observed by Braue and Pannella³ can be explained, at least in part, by simply studying the behavior of rays lying in an axial plane. In reality, all rays are to some degree skew rays (i.e., they are inclined to the nearest axial plane). We have carried out a computer ray trace analysis for various distributions of skew rays and found that, as long as the internal reflectance element and the two reflexicon systems are accurately positioned to be coaxial with each other and with the radiation distribution, the consideration of skew rays will not materially alter distribution of incidence angles at the analyte interface and hence will have little effect on the predicted nonlinear behavior. However, if any of these elements are not properly positioned, rays which are in an axial plane with respect to the focusing optics, for example, can be highly skewed with respect to the axis of the IRE. Some of these can follow paths through the element which are characterized by quite low incidence angles, in effect contributing stray light to the measurement. It seems likely that such rays contributed to the very marked nonlinearities observed by Braue and Pannella in some of their runs.³

Polarization Effects. A third optical effect which can lead to nonlinearity in internal reflectance spectroscopy is the dependence of effective sample thickness on optical polarization. However, unlike the effects treated in the above two sections, this effect is highly predictable.

The curves in Fig. 1 and Ref. 4 give the effective thickness (d_{\parallel}) for radiation with its electric field parallel to the plane of incidence. A second set of curves, also provided in Ref. 4, gives values of d_{\perp} , the effective thickness for radiation polarized in the orthogonal direction. These latter values are typically a factor -of-two smaller than those given in Fig. 1.

A computer ray trace analysis indicates that, for the design to be considered below, the planes of incidence of the majority of transmitted rays do not change materially as they propagate through the element. In this case, we can simply treat a ray as the superposition of two rays having electric fields parallel and perpendicular to this plane. In the case of randomly polarized input radiation, the net transmitted intensity will be the sum of the intensities for the two polarization states, and we can write the following expression for the net transmission:

$$T = (T_{\parallel} + T_{\perp}) / 2 = (10^{-n\alpha d_{\parallel}} + 10^{-n\alpha d_{\perp}}) / 2 \quad (1)$$

where α is the absorption coefficient and n is the number of reflections at the analyte interface.

The net absorbance is simply $A = -\log T$.

In the limit of very low absorbance, we can evaluate Eq. 1 by a series expansion. In this case, the limiting value of the net absorbance becomes

$$A_L = n\alpha (d_{\parallel} + d_{\perp}) / 2 \quad (2)$$

We can see from Eq. 1 that, under our assumptions, the polarization dependence is equivalent to a two-step transmission cell. Furthermore, its characteristics depend only on the indices of refraction of the element and the analyte and on the angle of incidence of the IR radiation. As long as the angle of

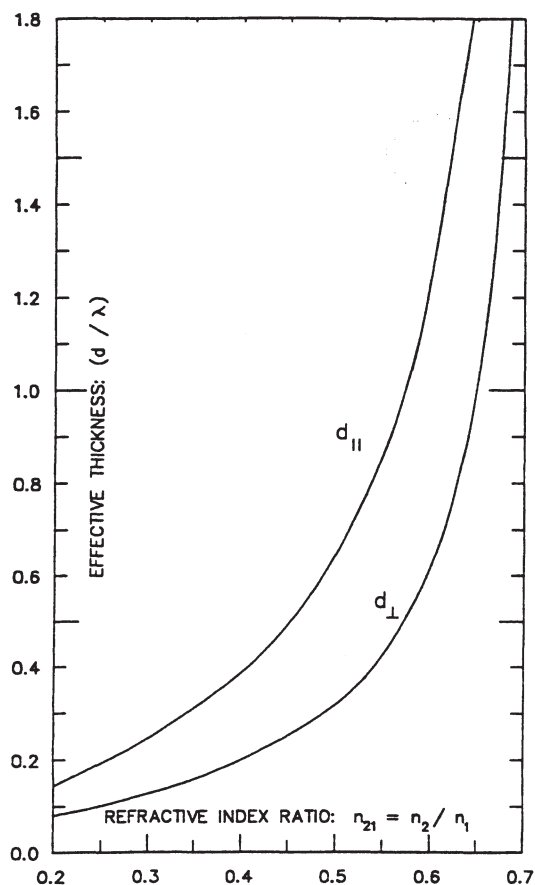


Fig 4. The dependence of the effective sample thicknesses, $d_{||}$ and d_{\perp} , on the refractive index ratio for the 45° incidence case. These curves, which are derived from Harrick's working curves (Ref. 4), can be used to evaluate the dependence of absorbance on concentration for mixtures of various substances.

incidence is well defined, the effect on measured absorbance values should be highly predictable and repeatable and thus should not be an impediment to accurate quantitative measurement. The magnitude of this effect is illustrated in Fig.3.

For a more complete analysis we would need to consider

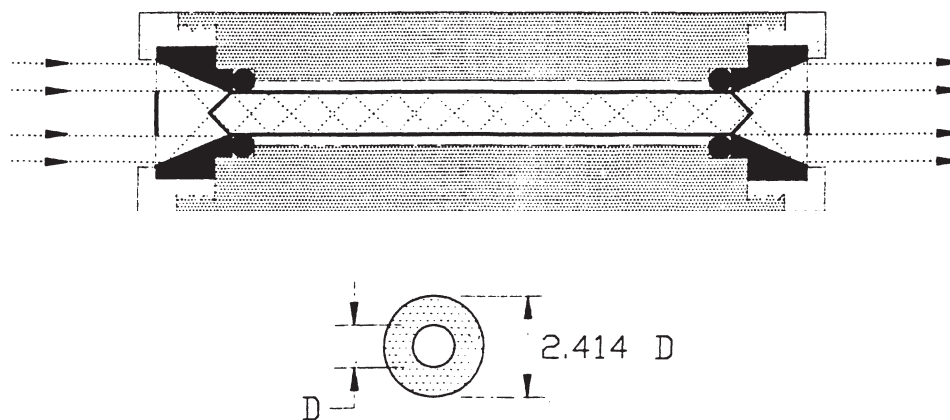


Fig 5. The design of a cylindrical internal reflectance (CIR) cell using 22.5° reflecting cones to redirect paraxial rays so that they strike the 45° end cone of the IRE at normal incidence and to redirect the output radiation. When used with collimated radiation, all rays will strike the analyte interface at 45° . The optical stops intercept rays which would otherwise enter the IRE without first striking the reflecting cone. The lower figure illustrates the image of the IRE entrance cone as viewed along the optical axis. "D" is the diameter of the IRE

the rotation of the plane of incidence of skew rays as they propagate through the element. The effect of this factor will be to reduce the magnitude of the effect discussed above.

Refractive Index Variations. As the working curves given in Fig. 1 and Ref. 4 illustrate, the effective sample thickness is dependent on the ratio between the refractive index of the analyte and that of the IRE. In a mixture of two substances having different refractive indices, this ratio will vary with the relative concentrations of the two substances. The result will be a quadratic contribution to the dependence of measured absorbance on concentration. The magnitude of this contribution can be estimated by using Harrick's working curves to generate approximate curves of effective thickness vs. refractive index for a given angle of incidence. Such curves are given in Fig. 4 for the 45° case.

The experiments to be described later in this paper used mixtures of acetone and water. The refractive indices of these two substances are reported to be 1.356 and 1.3325, respectively.⁷ In the appropriate region, the two curves of Fig. 4 have the following normalized slopes:

$$(1/d_{||}) dd_{||}/dn = 0.052 \text{ and } (1/d_{\perp}) dd_{\perp}/dn = 0.054$$

We thus would expect to see an approximately 5.3% positive change in effective thickness over the full range of concentrations from 0 to 100% acetone. For intermediate points, the contribution will be linear in concentration. As in the case of the polarization effect, this effect is stable and predictable and thus should not pose a problem.

3. An Improved Cylindrical Internal Reflectance Optical Design

In order to eliminate the unpredictable optical effects discussed in the first two sections, above we have developed a family of cylindrical internal reflectance sampling devices in which the transmitted rays propagate within a narrow range of angles within the internal reflectance element. The basic design is il-

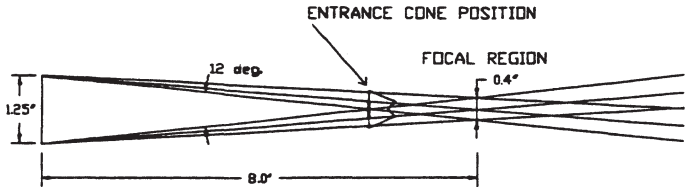


Fig 6. Distribution of extreme rays in a typical “focused beam” FT-IR sample compartment. The position of the entrance cone is shown for a cell using a 3.25-in.-long IRE centered in the sample compartment.

illustrated in Fig. 5 for the case of collimated input radiation. A key element of this design is the use of conical reflectors at the input and output of the internal reflectance element. The input cone reflects each paraxial ray so that it strikes the conical end surface of the element at approximately normal incidence. The output cone redirects the emerging cone of rays into the paraxial direction. In addition, stops located at the large end of each reflecting cone block any rays which would otherwise enter the rod without first being reflected from the cone.

A convenient way to visualize this situation is to consider the reflection of the rod’s entrance cone as viewed in the reflecting cone. The image will have the form of a flat annular disk with an inner diameter equal to the diameter of the rod and an outer diameter 2.412 times this diameter (see Fig. 2). The unusable inner area corresponds to roughly 17% of the total circular area.

An incoherent radiation beam is never perfectly collimated. However, by starting with nominally collimated radiation (i.e., a beam with the same angular divergence characteristics at each point in its wave front), the arrangement illustrated in Fig. 5 provides both the minimum possible divergence for a given optical throughput and a uniform distribution of ray coordinates at the entrance surface of the reflectance element. This latter characteristic renders the performance relatively insensitive to the positioning of the element. As a further refinement, however, the element can be supported by the same structure as the reflecting cones, with no allowance for relative movement.

If we assume perfectly collimated radiation and optical elements having ideal surface characteristics, the transmission of the sampling cell will be limited only by the area of its entrance aperture, the reflection losses at the rod entrance and exit surfaces (17% per surface), the reflection losses at the metal cones (3-4% each), and the area loss due to central obscuration and its supporting arms (typically 22%). Thus, with a beam diameter equal to the diameter of the cell’s entrance aperture, the theoretical transmission would be about 50%.

A nominally collimated beam obtained from an FT-IR spectrometer will have a spread of typically $\pm 1^\circ$. Virtually all of the individual optical rays will be skew rays in the sense that their propagation directions will be inclined to the nearest axial planes. We have carried out a computer ray trace analysis to determine the effects of given distributions of skew rays on cell performance. We found that, for a uniform distribution of spatial and angular ray coordinates with angles ranging up to $\pm 2^\circ$ in all possible directions, approximately 80% of the transmitted rays will fall within the initial angular distribution. If we assume that rays outside of this distribution would not be focused on the detector, we can take 80% as a worst case estimate of the transmission factor due to skew ray effects. Most of the rays that are lost have relatively large skew angles and either miss the tip of the cone or are excessively deflected on entering the cone near the tip.

Although collimated radiation was assumed for the above discussion, it is useful to estimate the performance to be obtained if the basic cell illustrated in Fig. 5 is used with the focused beam geometry typical of most commercial FT-IR spectrometers. As fig. 6 illustrates, the distribution of rays in the vicinity of a soft focus has much in common with the collimated case in the sense that it provides a roughly uniform spatial distribution of angular coordinates in the focal plane. If our sampling cell is centered in this place, most of the rays will fall within the area of its entrance cone. This is illustrated by the superimposed cone in Fig. 6.

For the beam geometry shown in Fig. 6, the total range of rays is about 12° . However, the range of incidence angles at the conical input surface of the internal reflectance element

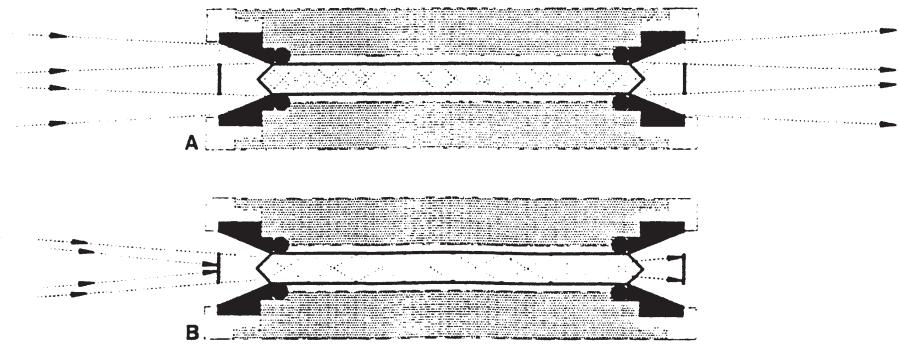


Fig 7. Operation of the new CIR cell design with a focused beam similar to that illustrated in Fig 6. Figure 7A illustrates the rays that are able to pass through the cell. These have a maximum divergence range of -2° to $+4^\circ$ relative to the cell axis, resulting in incidence angles at the analyte interface ranging from 44.17° to 46.65° . Rays making larger angles with the cell axis are blocked by either the input or the output stop, as illustrated by Fig. 7B.

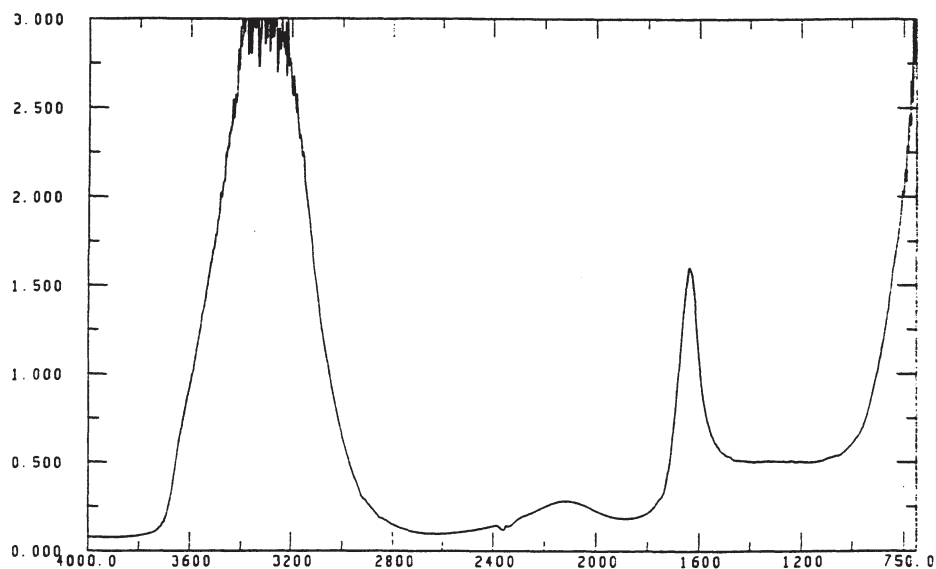


Fig 8. Absorbance spectrum of water obtained with a cell of the type illustrated in Fig. 5, utilizing a 3.25-in. long - 0.25" diameter IRE (11 effective reflections).

will be typically a factor-of-two less than this. This is due in part to the axial symmetry of the device combined with the fact that its input aperture is located in a converging beam. For example, all rays which have the same inclination to the axis will have the same incidence angle at the reflectance element even though they may form a sharply converging cone in space. In addition, the majority of the rays entering the cell at points along a given radius will be inclined towards the axis. For the case illustrated, the rays which fall within the annular entrance aperture will range from about -2° to $+4^\circ$. Rays which have larger angles of incidence will be blocked by either the input or the output stop, as illustrated in Fig. 7. For these conditions, the rays striking the analyte interface will be restricted to angles ranging from 44.17° to 46.65° .

To ensure that the distribution of incidence angles is minimized, it is only necessary to adjust the angular orientation of the cell in the spectrometer sample compartment for maximum transmission. Once this is done, the new CIR cell design should yield considerably greater depth of sample penetration and absorbance linearity than the earlier design illustrated in Fig. 2, even when used in a focused beam sample compartment.

The cell transmission to be expected with a given FT-IR spectrometer will depend on the particular, distribution of radiation in the spectrometer's sample compartment. In view of the wide variations in spectrometer designs, we have not attempted to calculate cell transmission in the focused case. However, we have operated the cells in spectrometers pro-

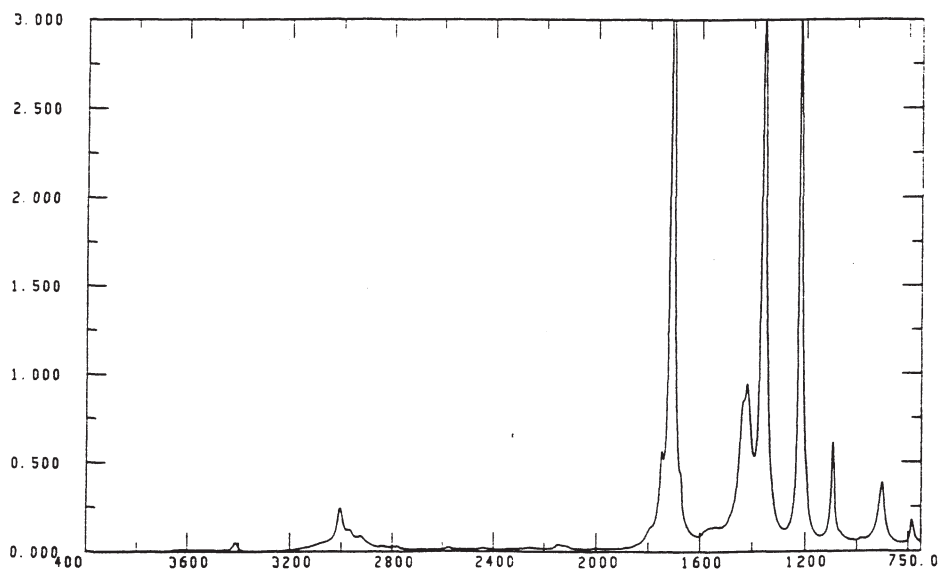


Fig. 9. Absorbance spectrum of acetone obtained with the same cell as Fig. 8. Note that both of these spectra exhibit absorbance values which are 2.5 to 3 times greater than those typically observed with earlier CIR cell designs.

TABLE I. Measured peak absorbance of the 1220-cm⁻¹ acetone band vs. percent concentration of acetone in water for data gathered 1/10/89 using the Analect RFX-40 FT-IR.

| % Acetone by volume | Absorbance | Linear calibration factor (ratio) |
|-------------------------|------------|-----------------------------------|
| 75 | 1.96 | 2.61 |
| 50 | 1.34 | 2.68 |
| 25 | 0.70 | 2.80 |
| 10 | 0.30 | 3.00 |
| 5 | 0.16 | 3.20 |
| 2.5 | 0.07 | 2.80 |
| Mean calibration factor | | 2.82 |
| Standard deviation (SD) | | 0.16 |
| Normalized SD | | 5.7% |

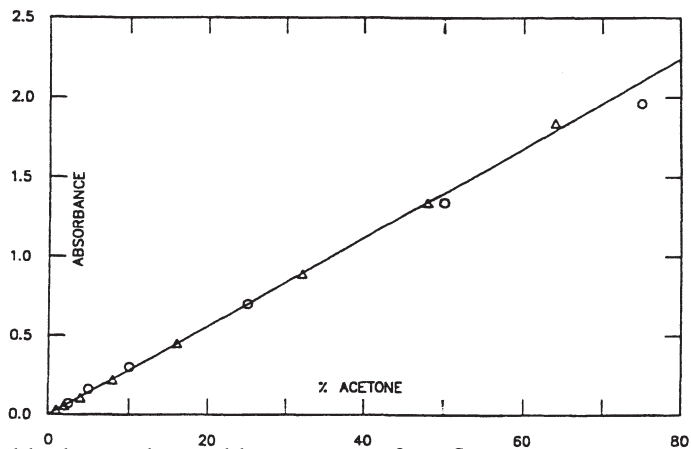
duced by six different manufacturers and have obtained transmission values ranging from 17% to over 30%.

4. Experimental Observations

The data reported below were gathered with the use of two different FT-IR spectrometers, an Analect RFX-40 using a room-temperature pyroelectric detector and a Bomem Michelson 110 using a cooled HgCdTe detector. In each case, the standard focused beam sample compartment was used. The internal reflectance cell corresponded to the design illustrated in Fig. 5 and used a 3.25-in. long, 0.25-in.-diameter ZnSe element, yielding eleven reflections at the element/analyte interface. For comparison, the cell used by Braue and Panella³ employed a 1.5-in. long, 1/8-in.-diameter rod and was prob-

Table II. Measured peak absorbance of the 1220-cm⁻¹ acetone band vs. percent concentration of acetone in water for data gathered 2/27/89 using the Bomem Michelson 110 FT-IR.

| % Acetone by volume | Absorbance | Linear calibration factor (ratio) |
|-------------------------|------------|-----------------------------------|
| 64 | 1.84 | 2.88 |
| 48 | 1.34 | 2.79 |
| 32 | 0.89 | 2.78 |
| 16 | 0.45 | 2.81 |
| 8 | 0.22 | 2.75 |
| 4 | 0.105 | 2.63 |
| 2 | 0.056 | 2.80 |
| 1 | 0.029 | 2.90 |
| Mean calibration factor | | 2.79 |
| Standard deviation (SD) | | 0.077 |
| Normalized SD | | 2.76% |



ably designed to yield an average of 9 reflections. Fig. 10. Peak height measurements for the 1220-cm⁻¹ band of acetone as a function of concentration of acetone in water. The circles represent data taken on an Analect RFX-40. The triangles represent data taken on a Bomem Michelson 110 after the cell was modified to improve its transmission. In each case, the cell was simply positioned in the sample compartment for maximum transmission. No other adjustments were made.

In order to provide a direct comparison with the data of Braue and Pannella,³ we studied the same acetone band (1220cm⁻¹) used in their work. For each data point, an appropriately scaled water spectrum was subtracted from the spectrum of the mixture. Corrected peak height values were then obtained by subtracting a local baseline absorbance (interpolated between 1140 and 1272 cm⁻¹) from the measured peak absorbance. We did not calculate peak areas.

Absorbance spectra of pure water and pure acetone are shown in Figs. 8 and 9, respectively. The most notable features of these spectra are the intensities of the bands, with absorbance values between two and a half and three times higher than those obtained by Braue and Panella.³ For example, the broad water band centered at 3300 cm⁻¹ was found to have height of approximately three absorbance units, as opposed to approximately one for their data.³ In fact, on comparing spectra of various substances obtained with the new design to published spectra obtained with previous cylindrical internal reflectance design (Ref. 7), we typically obtain 2.7 times greater absorbance values for a given number of reflections. This is an even greater enhancement than we had predicted on the basis of our analysis of the theoretical ray distributions in the two cell designs.

Tables I and II and Fig. 10 include all of the data taken during two separate sets of experiments, one carried out on 10 January 1989 with the Analect Spectrometer and the other on 27 February with the Bomem. Between the two measurement sessions, the cell structure was shortened about 1 mm to compensate for the fact that the element being used was shorter than specified. This modification approximately doubled the cell transmission to a value of roughly 20%. A further difference between the two sets of experiments is the fact that the

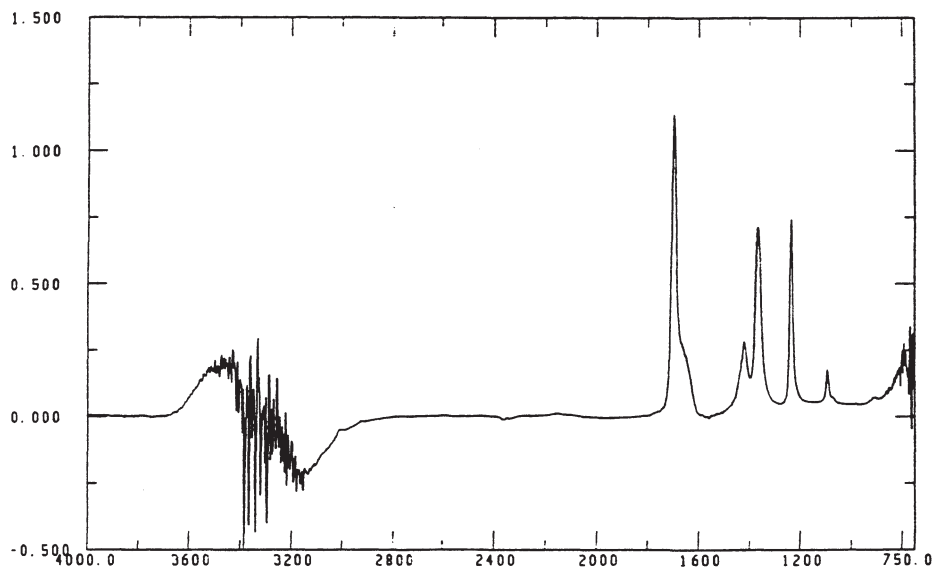


Fig. 11. Spectrum of 25% mixture of acetone in water after subtraction of an appropriately scaled water spectrum. Chemically induced shifts in the water spectrum are evident in three regions of the spectrum.

mixtures were prepared with greater care for the second set, with a fresh mixture being prepared immediately before each spectral acquisition. After each measurement, the cell was removed from the sample compartment, emptied, and dried with a flow of warm air.

The data given in the two tables and in Fig. 10 have two important characteristics. First, we observed no measurable non-linearity, even with a 75% acetone mixture. Second, and more important, the two sets of data fall on the same straight line, to well within the experimental uncertainty. This response occurred despite the modifications made to the cell between the

two sets of experiments and the substantially different beam geometry of the two instruments used. This result tends to confirm our expectation that a given cell would be characterized by a calibration determined only by the length of its reflectance element and its permanent mechanical structure and that absorbance measurements would be relatively independent of the distribution of IR radiation in the spectrometer sample compartment. This supposition was further supported by experiments in which cells were purposely misaligned in the sample compartment. We were able to produce absorbance errors as high as 6% or 7% by grossly misorienting a cell. However, a small amount of care in positioning a cell

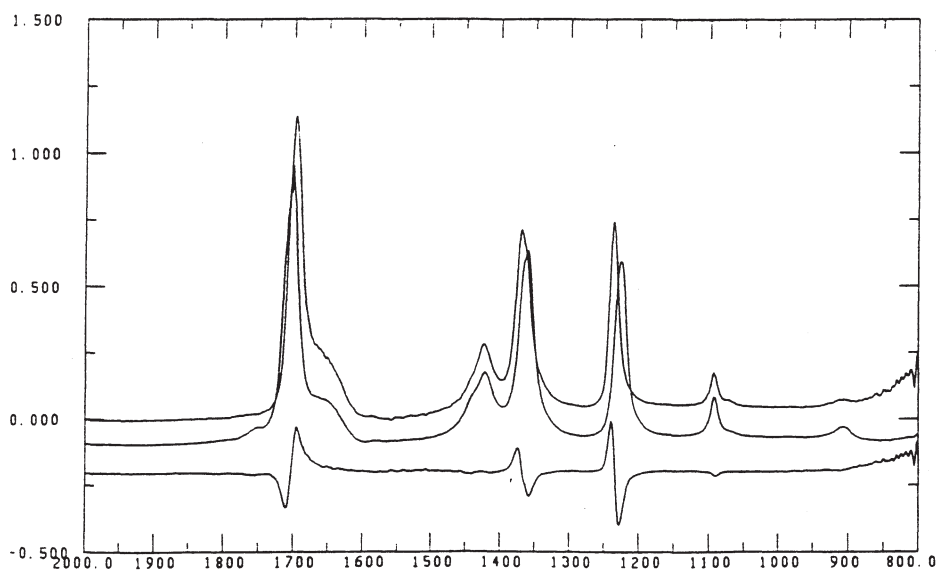


Fig.12. Spectral comparison of 25% and 50% concentrations of acetone in water. The upper trace corresponds to an expanded region of the 25% acetone spectrum Fig. 11. The middle trace is a 50% acetone spectrum with the absorbance values divided by three and displaced downward for clarity. The lower trace is the difference between the upper two. For this system, chemical interactions have a more obvious effect on band frequencies than on intensities.

TABLE III. Measured peak absorbance vs. concentration for the five strongest bands of acetone. Data taken 3/10/89 using the Bomem Michelson 110.

| % Acetone by volume | Absorbance for indicated band (in cm^{-1}) | | | | |
|---------------------|--|-------|-------|-------|-------|
| | 1715 | 1425 | 1357 | 1220 | 1092 |
| 6 | 0.34 | 0.058 | 0.171 | 0.182 | 0.026 |
| 12 | 0.64 | 0.126 | 0.337 | 0.345 | 0.052 |
| 20 | 1.13 | 0.202 | 0.570 | 0.596 | 0.098 |
| 30 | ... | 0.307 | 0.836 | 0.862 | 0.179 |
| 30 (repeat) | ... | 0.324 | 0.874 | 0.848 | 0.156 |
| 42 | ... | 0.441 | 1.23 | 1.22 | 0.236 |
| 50 | ... | 0.537 | 1.45 | 1.42 | 0.293 |
| 55 | ... | 0.590 | 1.56 | 1.54 | 0.315 |
| 60 | ... | 0.679 | 1.83 | 1.82 | 0.377 |

to maximize the IR signal (say, within 20%) typically yielded absorbencies within 3% of the expected values.

The excellent linear fit obtained in the above experiments is somewhat surprising in view of the predicted nonlinear contribution due to polarization dependence. As indicated by Fig. 3, we would expect to see a 20% negative departure from linearity at two absorbance units. For mixtures of acetone and water, the index of refraction effect will be in the opposite direction from the polarization effect. However, for this mixture the effect is quite weak, amounting to only a 3% positive contribution at a 60% acetone concentration. At this point, we can only speculate that the expected negative nonlinearity

TABLE IV. Linear calibration factors, LCF (Abs/Concentration) for the five strongest bands of acetone. Values derived from Table III.

| % Acetone by volume | LCF for indicated band (in cm^{-1}) | | | | |
|---------------------|---|-------|-------|-------|-------|
| | 1715 | 1425 | 1357 | 1220 | 1092 |
| 6 | 5.63 | 0.97 | 2.85 | 3.03 | 0.44 |
| 12 | 5.38 | 1.05 | 2.81 | 2.87 | 0.43 |
| 20 | 5.65 | 1.01 | 2.85 | 2.98 | 0.49 |
| 30 | ... | 1.02 | 2.79 | 2.87 | 0.60 |
| 30 (repeat) | ... | 1.08 | 2.91 | 2.83 | 0.52 |
| 42 | ... | 1.05 | 2.91 | 2.90 | 0.56 |
| 50 | ... | 1.07 | 2.91 | 2.84 | 0.59 |
| 55 | ... | 1.07 | 2.84 | 2.79 | 0.57 |
| 60 | ... | 1.13 | 3.04 | 3.03 | 0.63 |
| Mean LCF | 5.56 | 1.05 | 2.88 | 2.91 | 0.54 |
| Standard deviation | 0.12 | 0.043 | 0.071 | 0.083 | 0.066 |
| Normalized SD | 2.2% | 4.1% | 2.5% | 2.8% | 12.3% |

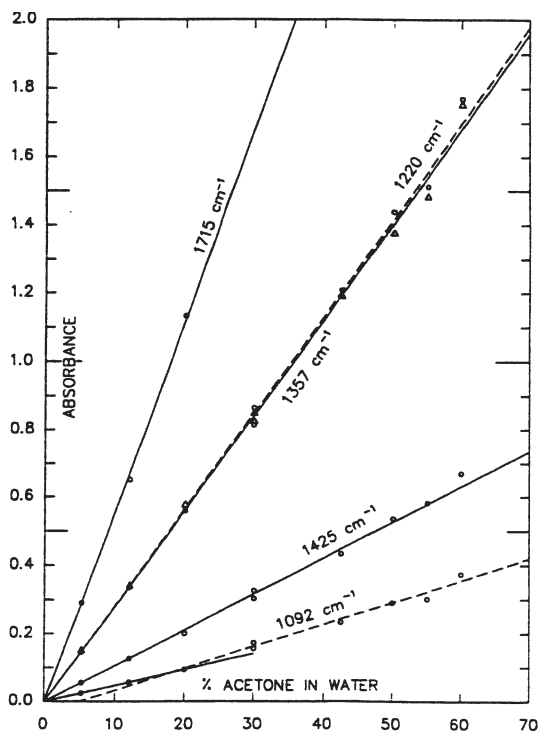


Fig. 13. Peak absorbance measurements for the five strongest bands of acetone. The absorbance values were obtained from a series of nine spectra corresponding to concentrations ranging from 6% to 60% acetone. The four strongest bands appear to be linear within the experimental uncertainty. The fifth appears to have an inflection at about 15% concentration.

due to polarization may be masked by a chemically induced positive nonlinearity of comparable magnitude.

Braue and Pannella observed significant frequency shifts in the various acetone bands as a function of concentration, indicating the presence of chemical interactions between the two species.³ These shifts were also clearly evident in the difference spectra used to obtain our peak height data. In Fig. 11, for example, the derivative characteristics evident at each side of the broad water band are an indication that this band has been shifted by the presence of acetone. Figure 12 illustrates the differential shifts of the acetone bands that occur with a change in concentration. Clearly, for this particular mixture, chemical interactions have a much more noticeable effect on peak frequencies than on peak heights. For many mixtures we would expect to encounter significant chemically induced nonlinearities in measurements of absorbance vs. concentration. However, these effects will generally be repeatable and easily characterized and thus should not be an impediment to the use of cylindrical internal reflectance for precise quantitative analysis.

The subtraction results illustrated in Fig. 12 suggest that the heights of the three strongest acetone bands are approximately proportional to concentration. In view of the fact that the results obtained with the 1220- cm^{-1} band were even more linear than expected, it seemed appropriate to study all of the strong acetone bands to see whether this result was purely accidental.

It should be noted, of course, the strongest band, (at 1715 cm^{-1}) overlaps a relatively unstable water band, so we did not attempt to take data at very low concentrations. Accordingly, we obtained a new set of 9 spectra using the Bomem spectrometer with very carefully prepared acetone concentrations ranging from 6% to 60%. The results are given in Tables III and IV and Fig. 13 for the five strongest bands.

Remarkably, all four of the strongest acetone bands were found to follow Beer's law to within the experimental uncertainty. Note that the normalized standard deviations listed in Table IV indicate an experimental accuracy of about 3% for individual measurements. Only the lowest three points were included in our analysis of the strongest band since our experience has indicated that, with the particular HgCdTe detector being used, bands with absorbance values over 2, prior to water subtraction, are relatively inaccurate.

The mean linear calibration value of 2.91 obtained for the 1220-cm^{-1} band is about 3% higher than the value obtained during the February 27 tests. This difference is probably due to the fact that the cell was modified between the two tests to incorporate improved reflecting cones and tighter alignment between the axes of the cones and the IRE.

The fifth strongest band (centered at 1092 cm^{-1}) did show some nonlinearity, as evidenced by the relatively large standard deviation in the linear fit provided in Table IV. Empirically, we found that the data for this band would fit a model incorporating two linear segments, with an inflection at about 15% concentration, as illustrated in Fig. 13. No attempt has been made to interpret this result. The remarkable fact is not that the 1092 cm^{-1} band is nonlinear, but rather that the four strongest bands of this system probes to be quite linear.

Needless to say, compliance with Beer's law should be regarded as the exception rather than the rule in mixtures of interacting substances. For example, we recently carried out a series of experiments using dilutions of methanol in water and, as expected, observed significant nonlinearities. The important point is not whether a given system is linear or not, but whether one can obtain accurate, repeatable data under a wide variety of experimental conditions.

5. Conclusions

The experimental results reported above have demonstrated that an optimized optical design will result in three significant enhancements to cylindrical internal reflectance spectroscopy: (1) an increase in absorbance peak heights by a factor typically between 2.5 and 3, (2) calibration which is a fixed characteristic of a given cell, rather than being dependent on optical adjustments or the distribution of radiation in the sample compartment, and (3) the minimization of optically induced nonlinearities.

We also found that, for a mixture of acetone and wa-

ter, the new CIR cell design can yield a high level of absorbance linearity and repeatability. It should be noted, however, that sources of nonlinearity other than improper optical design may become significant for some experimental conditions. In particular, variations in refractive index will be significant for mixtures of substances having disparate indices, and the linearity of the internal reflectance phenomenon itself will break down for very highly absorbing samples. Polarization effects, chemical interactions, and instrument resolution should also be significant in some situations. However, each of these effects should probe stable and thus can be characterized and accounted for in a given situation. On the other hand, the dependence of measured absorbance on angle of incidence and number of reflections can give rise to measurements which are both nonlinear and highly dependent on the optical adjustment of the sampling cell. The new design described above has eliminated this problem.

Acknowledgements

I would like to thank Bruce McIntosh of Laser Precision Analytical for his assistance with the experiments performed on the Analect RFX-40, and Bomem, Inc. for the generous loan of the Michelson 110 used in the later experiments.

References

1. Paul Wilks, Jr., Industrial Research and Development, Sept. 132 (1989).
2. "Prism Liquid Cell," Data Sheet #10 (Harrick Scientific Corporation, Ossining, New York).
3. Ernest H. Braue, Jr. and Michael G. Pannella, *Appl. Spectrosc.* **41**, 1057 (1987).
4. N.J. Harrick, *Internal Reflection Spectroscopy* (John Wiley, New York, 1967)
5. Tomas Hirschfeld, in *Fourier Transform Infrared Spectroscopy*, J.R. Ferraro and L.J. Basile, Eds. (Academic Press, New York, 1979), Vol. 2, pp. 215-221..
6. W. R. Rambausk, U.S. Patent No. 3,827,059 (1974).
7. *Sprouse Collection of Infrared Spectra*, Book II: *Solvents by Cylindrical Internal Reflection*, Diana L. Hansen, Ed. (Sprouse Scientific Systems, Inc., Paoli, Pennsylvania, 1987).